Surface & Coatings Technology 205 (2010) 1415–1419

Contents lists available at ScienceDirect

Surface & Coatings Technology

journal homepage: www.elsevier.com/locate/surfcoat

Numerical study of tensile tests conducted on systems with elastic-plastic films deposited onto elastic-plastic substrates

N.K. Fukumasu [a,*], C.M. Angelo [a], M. Ignat [b], R.M. Souza [a]

[a] Polytechnic School, University of Sao Paulo, Sao Paulo, Brazil
[b] DFI, FCFM, University of Chile, Santiago, Chile

ARTICLE INFO

Available online 5 August 2010

Keywords:
Thin film mechanics
Crack geometry
FEM
Computer simulation
Stress distribution
Fracture

ABSTRACT

In this work, a series of two-dimensional plane-strain finite element analyses was conducted to further understand the stress distribution during tensile tests on coated systems. Besides the film and the substrate, the finite element model also considered a number of cracks perpendicular to the film/substrate interface. Different from analyses commonly found in the literature, the mechanical behavior of both film and substrate was considered elastic-perfectly plastic in part of the analyses. Together with the film yield stress and the number of film cracks, other variables that were considered were crack tip geometry, the distance between two consecutive cracks and the presence of an interlayer. The analysis was based on the normal stresses parallel to the loading axis (σ_{xx}), which are responsible for cohesive failures that are observed in the film during this type of test. Results indicated that some configurations studied in this work have significantly reduced the value of σ_{xx} at the film/substrate interface and close to the pre-defined crack tips. Furthermore, in all the cases studied the values of σ_{xx} were systematically larger at the film/substrate interface than at the film surface.

1. Introduction

The straining in uniaxial tension is a useful method to study the mechanical behavior of films on substrates [1–15]. Usually, when this type of test is applied to coated systems, a sequence of events is observed [4–6]. The straining of the system above a given critical value results in the propagation of an initial network of transverse cracks in the film, which are defined [5] as primary cracks. The straining of the system further above the critical value usually leads to a rapid increase in the number of primary cracks, i.e. an increase in transverse crack density. With even further straining, the increase in crack density slows down and reaches a saturation value with no further transverse crack propagation. As an additional stage of these tensile tests, film decohesion and buckling may occur for strips of the film that are located in-between two successive transverse cracks [2,7,12].

The continuous interest on this experimental technique indicates the importance of the correct understanding of the distribution of the stresses responsible for film failure. To improve the comprehension of those distributions, both analytical [1,2,4–7,12–14,16] and the finite element method (FEM) have been selected to analyze the stresses and strains in coated systems subjected to tensile loads [16–21], from tensile [16–20] or four-point bending tests [21]. Usually, results are analyzed based on the normal stresses parallel to the loading axis (σ_{xx}), which are responsible for the transverse cracks that are observed in the film. Although centered on the same basic geometry, many alternatives were considered in literature work, in order to reproduce the conditions found in practice. These alternatives include the presence of an interlayer between the film and the substrate [19], variations in crack geometry at the crack tip [16–18] and the consideration of a small debonded area along the interface and close to the transverse crack tip [18]. In general, the FEM analyses provide good agreement with those obtained analytically, in terms of the shape of the distribution of σ_{xx} in the region between two consecutive transverse cracks. On the other hand, in some cases, FEM analyses present two features that are not seen in analytical results: (i) larger σ_{xx} stresses at the film/substrate interface than at the film surface and (ii) a peak in the distribution of σ_{xx} along the interface, located close to the transverse crack tip. For example, if the ratio λ between transverse crack spacing and film thickness is equal to 20, this peak is located approximately at 10% of the length between two cracks [18,19].

In this work, the alternatives mentioned above were considered in the preparation of a series of FEM simulations of tensile tests in coated systems. The main objective was to analyze the effect of these alternatives on the distribution of σ_{xx} stresses and, consequently, on their ability to explain the phenomena observed experimentally.

2. Model description

This work was based on 2D parametric analyses, which were conducted on the Abaqus® finite element environment. The systems

* Corresponding author.
E-mail address: newton.fukumasu@gmail.com (N.K. Fukumasu).

0257-8972/$ – see front matter © 2010 Elsevier B.V. All rights reserved.
doi:10.1016/j.surfcoat.2010.07.104

were solved in a mechanical equilibrium state of the applied loads. No time derivatives were considered in this work.

2.1. Geometric and mesh parameters

Fig. 1 presents the geometry analyzed in this work, in which h_s is the height of the substrate, h_f is the film thickness, d_s is the width of the substrate and d_c is the distance between two consecutive cracks. The global orthogonal coordinate system is also presented. All the cases analyzed in this work considered a film thickness of $h_f = 4\,\mu m$, a height and a width of the substrate of $h_s = 400\,\mu m$ and $d_s = 800\,\mu m$, respectively.

Additionally, Fig. 1 shows three predefined cracks through film thickness, perpendicular to the film/substrate interface. Those cracks were always positioned symmetrically with respect to the width d_s. Either two or three cracks were considered in the simulations and, for the cases with only two cracks, crack c_2 was suppressed.

An element size of $0.01\,\mu m$ was applied uniformly in the discretization of the region near the crack tip in all cases. A total of about 120,000 structured quadrilateral elements were used to discretize the computational domain in order to obtain mesh independent results. All elements were based on the plane strain theory with 8-node biquadratic interpolation.

2.2. Parametric analyses

The cases studied in this work were based on four parameters: the dimensionless distance λ, defined as the ratio between the distance d_c and the film thickness (h_f), the yield stress of the film (σ_f), the crack tip geometry and the presence of an interlayer between the film and the substrate.

Fig. 2 shows a schematic of the crack tip geometries analyzed in this work. A single node sharp crack in the film/substrate interface (Fig. 2a) is the simplest choice to represent a 2D crack front. However, this option tends to create a point of numerical singularity, deteriorating the stability of the numerical solution [18]. The dual node tip allows analyses with two other geometries of crack tip: fully opened cracks (Fig. 2b) and small debonding of the film/substrate interface at the transverse crack tip (Fig. 2c). For the cases with two nodes in the crack tip, the total length d_{c1} of the interface debonding and the predefined opened crack size (Fig. 2) was $0.2\,\mu m$. All those crack tip configurations were based on general geometries discussed in the literature, including [17,18,25–27]. Some of these geometries were also observed experimentally, especially fully opened cracks [14,18]. Similarly, the values of λ selected in this work are representative of both situations analyzed in the literature and those seen during experiments.

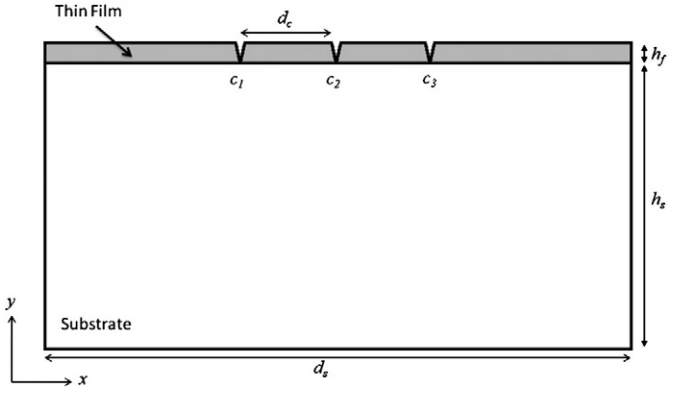

Fig. 1. General parameters of the geometry: h_s — height of the substrate, h_f — film thickness, d_s — width of the substate and d_c — distance between two consecutive centered cracks.

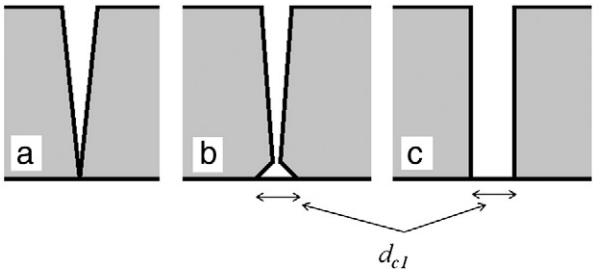

Fig. 2. Schematics of the crack tip regions analyzed in this work: a) single node sharp crack; b) two nodes with small debonding of the interface (⊥); c) two nodes with fully opened cracks (⊔).

Table 1 presents the analyses that were conducted. The combination of the parameters generated a total of 19 simulations. In this table, the symbol ⊥ represents the crack tip with small interface debonding and ⊔ denoted the fully opened crack tip.

2.3. Material modeling

The substrate was considered elastic-perfectly plastic. As indicated in Table 1, for part of the analyses, the behavior of the film was also based on the elastic-perfectly plastic model. For both film and substrate, the Von Mises criterium was selected to indicate the onset of the plastic regime.

The material properties were selected similar to Krishnamurthy and Reimanis [18] who worked with CrN films on brass. The substrate was modeled with an elastic modulus of 110 GPa, a Poisson coefficient of 0.3 and an yield stress of 189 MPa. For the thin film, the elastic modulus and the Poisson coefficient were, respectively, 380 GPa and 0.25. The yield stress of the film, when needed, was selected as 6000 MPa [22].

Additionally, the material of the interlayer (with a thickness of $0.50\,\mu m$) between the film and substrate was defined with an elastic modulus of 116 GPa, a Poisson coefficient of 0.34 and an yield stress of 140 MPa, which are common values for pure titanium [23]. Note that it may not be usual to have a Ti interlayer with a CrN film, but these values were selected to keep the interlayer properties close to those of the substrate, instead of selecting values in the middle range of the film and the substrate.

2.4. Boundary conditions

To represent a tensile test, the system presented in Fig. 1 was submitted to a predefined displacement in the x-direction, parallel to the film/substrate interface. The bottom of the domain was constrained with a symmetric condition, normal to the y-axis.

A displacement, representing a strain of 1%, was applied at the boundaries of the substrate. This strain value, which is consistent with those observed prior to the crack saturation stage in actual tests [8,12,14], was selected in a way to maintain both the convergence and stability of the numerical solution.

The interface between two distinct materials was modeled as perfectly bonded and neither slip nor crack nucleation were allowed. Also, no film residual stresses were accounted for in the analyses.

Table 1
Definition and ranges of the parameters analyzed in the numerical simulations.

Case	Number of cracks	Normalized crack distance (λ)	Film yield stress [MPa]	Crack tip points	Interlayer thickness
Baseline	2 and 3	5, 10 and 15	$+\infty$	1	–
Case 1	2 and 3	5, 10 and 15	6000	1	–
Case 2	2	5, 10 and 15	$+\infty$	2 ⊥ and ⊔	–
Case 3	2	5, 10 and 15	6000	1	0.5 μm

3. Results

Figs. 3, 4, 5 and 7, were organized similarly: filled symbols denote stress distribution at the film/substrate interface, unfilled symbols represent the region located at the film surface. Squares, circles and triangles represent λ values equal to 5, 10 and 15, respectively.

Fig. 3 presents the distribution of normal stresses (σ_{xx}) along the normalized distance between two consecutive cracks for baseline cases with two (Fig. 3a) and three (Fig. 3b) perpendicular cracks. As shown in this figure, an increase in the distance between cracks (λ) results in an increase in the stresses at the film surface and a decrease in the stresses at the film/substrate interface.

Fig. 3 also indicates that, far from the predefined cracks (intermediate values of x/d_c), the stress values at the surface become close to the values at the interface, especially as λ increases. This result

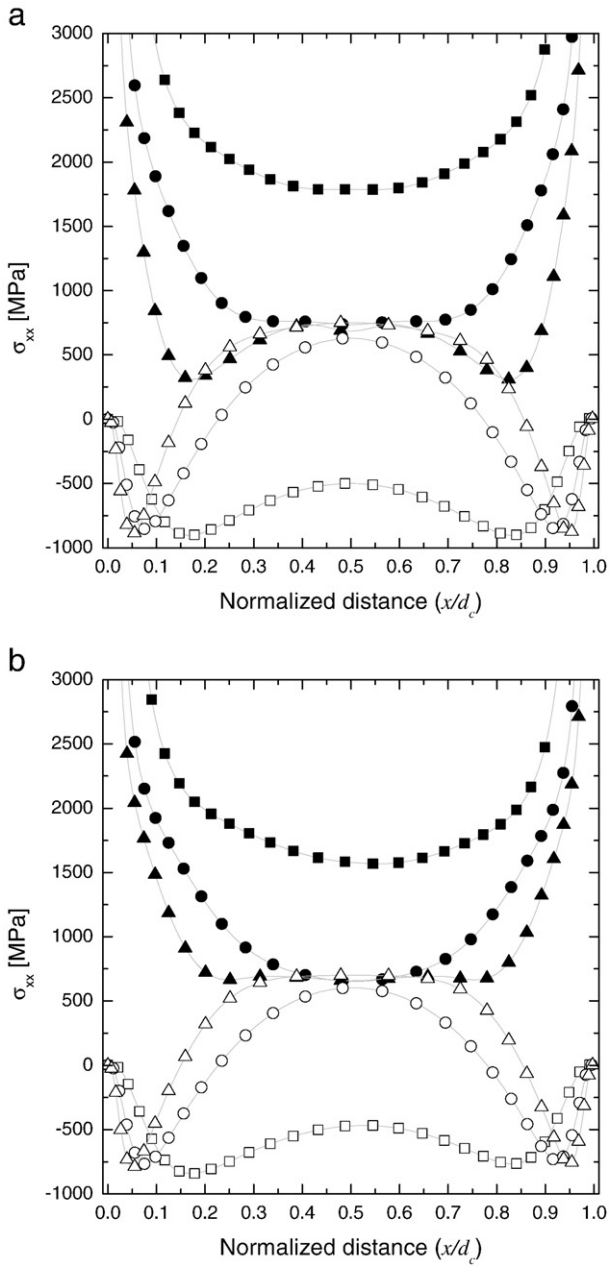

Fig. 3. σ_{xx} stress distribution between two consecutive cracks for the baseline case with two (a) and three (b) perpendicular cracks in the film: unfilled symbols - stress distribution at the film surface; filled symbols — stress distribution at the film/substrate interface; square — **λ = 5**; circle — **λ = 10** and triangle — **λ = 15**.

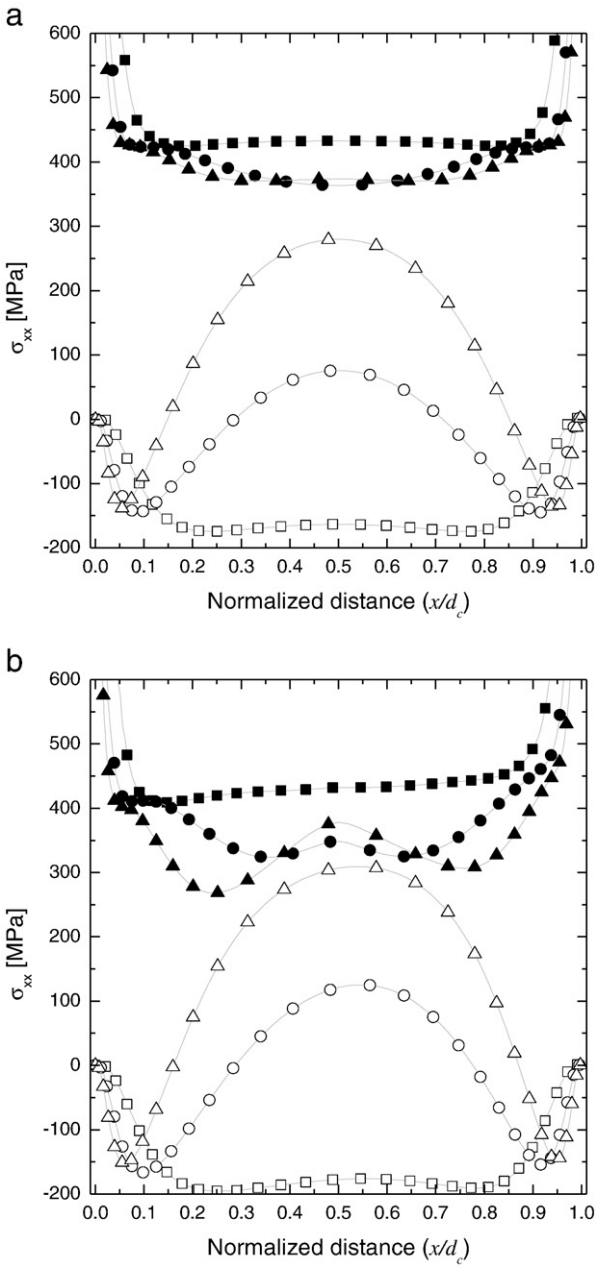

Fig. 4. σ_{xx} stress distribution for cases with two (a) and three (b) perpendicular cracks and film plasticity modeling: unfilled symbols — stress distribution at the film surface; filled symbols — stress distribution at the film/substrate interface; square — **λ = 5**; circle — **λ = 10** and triangle — **λ = 15**.

suggests that larger values of λ would provide more uniform distributions of σ_{xx} stresses along the film thickness, as assumed in the formulation of many analytical analyses [2,6,13,16] of the straining of coated systems in uniaxial tension. Close to the predefined cracks ($x/d_c \cong 0$ or $x/d_c \cong 1$), the stresses at the interface reach large tensile values, whereas the stresses at the surface are compressive.

Carefull observation of Fig. 3 also indicates that the introduction of a third crack (Fig. 3b) in the finite element model results in a slight asymmetry in the distribution of σ_{xx} stresses. These values become slightly more tensile at $x/d_c \cong 1$, which corresponds to the location of the central crack (c_2 in Fig. 1).

3.1. Influence of the film plasticity

Fig. 4 presents the σ_{xx} stress distribution for the cases with the film modeled as an elastic-perfectly plastic material. A significant reduction in

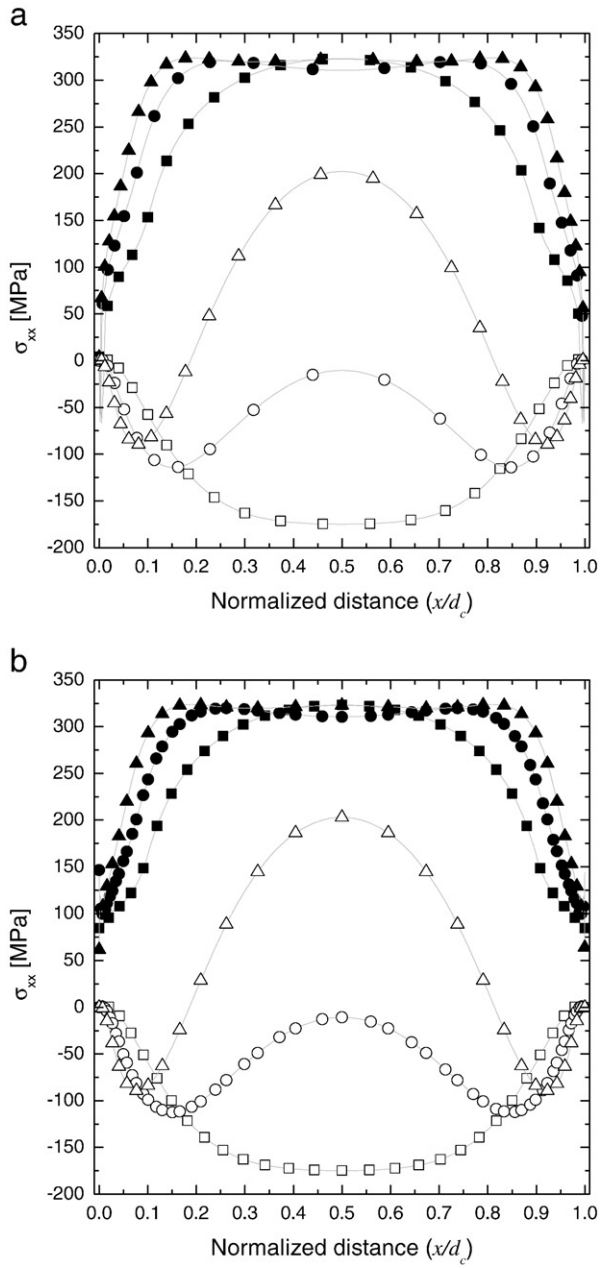

Fig. 5. σ_{xx} stress distribution between two consecutive cracks for the case with (a) small interface debonding and (b) fully opened crack tips: unfilled symbols — stress distribution at the film surface; filled symbols — stress distribution at the film/substrate interface; square — $\lambda = 5$; circle — $\lambda = 10$ and triangle — $\lambda = 15$.

σ_{xx} stresses was observed in these cases. Values at the interface remained more tensile than at the surface and the asymmetry in stress distribution due to the presence of a third crack (Fig. 4b) became more evident. Fig. 4 also indicates that the stresses at the surface and at the interface are no longer similar, which indicates less uniformity in σ_{xx} stress distribution along the film thickness. Furthermore, it is possible to note that the presence of a third crack was responsible for higher oscillations of stresses for higher values of λ and that values far from the predefined cracks, either tensile of compressive, are approximately one order of magnitude lower than the value of yield stress selected for the film.

3.2. Influence of crack tip geometry

Fig. 5a shows the σ_{xx} stress distribution for the case with two cracks presenting a small debonded area close to the tip (Fig. 2b). Fig. 5b refers to the fully opened crack tip geometry (Fig. 2c). Both figures indicate a reduction in stress values with respect to those from the baseline analysis (Fig. 3), as well as a loss in the uniformity of σ_{xx} stresses along the film thickness. Additionally, the stress distribution at the film/substrate interface presented almost the same maximum value for all λ. When the stresses along the interface are looked in more detail, it is possible to observe that, for $\lambda = 10$ and 15, the maximum value of σ_{xx} is not located in the middle ($x/d_c = 0.5$) of the two preexisting cracks, but closer to the cracks. This peak in stress distribution has already been observed in the literature [18,19] and Fig. 5 indicates that it gradually moves to $x/d_c = 0.5$ as λ increases.

Fig. 5 also indicates a suppression of the trend for infinite tensile stresses at the interface and close to the predefined cracks, as seen in Figs. 3 and 4. This statement is confirmed in Fig. 6, which presents a detail of the distribution of σ_{xx} stresses close to a crack tip. In this figure, filled symbols represent the small interface debonding case, whereas crossed symbols refer to the fully opened crack tip model. Moreover, Fig. 6 indicates that the difference in crack tip geometry affected only the stress distribution near the crack tips ($x/d_c < 0.1$), i.e. the distribution of σ_{xx} stresses is equal in Fig. 5a and b for $0.1 < x/d_c < 0.9$.

3.3. Influence of the interlayer

Fig. 7 presents the distribution of σ_{xx} stresses in the case where an interlayer was considered between the film and the substrate. The similarities between Figs. 5 and 7 indicate that the effect of the interlayer was similar to that obtained with the crack geometries shown in Fig. 2b and c.

4. Discussion

Usually, the studies of the distribution of stresses during the uniaxial straining of coated systems are focused on the distribution of the σ_{xx} stresses at the film surface, between two transversal cracks. The same general trends are usually observed in those analyses, either analytical or by the finite element method. In general, as indicated in the results of this work (Figs. 3–5 and 7), more tensile σ_{xx} stresses are observed at the surface as the spacing between cracks increases. As

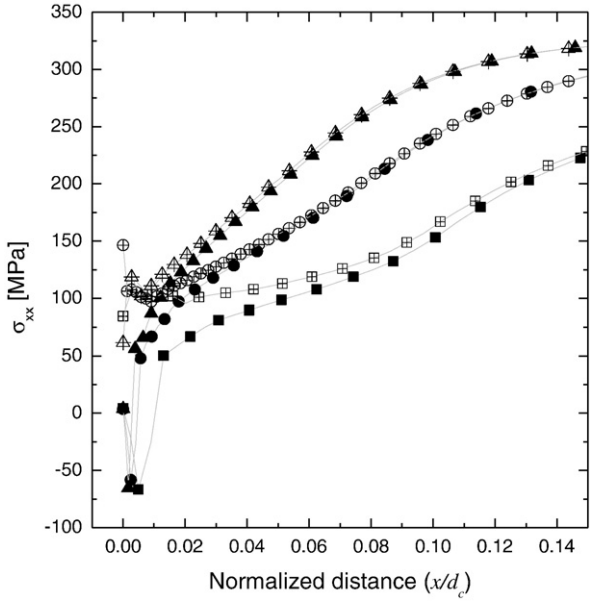

Fig. 6. Comparison of the stress distribution, at the film/substrate interface, between the case with the small interface debonding and the fully opened crack tips: filled symbols — stress distribution for small interface debonding at the crack tip; unfilled crossed symbols — stress distribution for the fully opened crack tips; square — $\lambda = 5$; circle — $\lambda = 10$ and triangle — $\lambda = 15$.

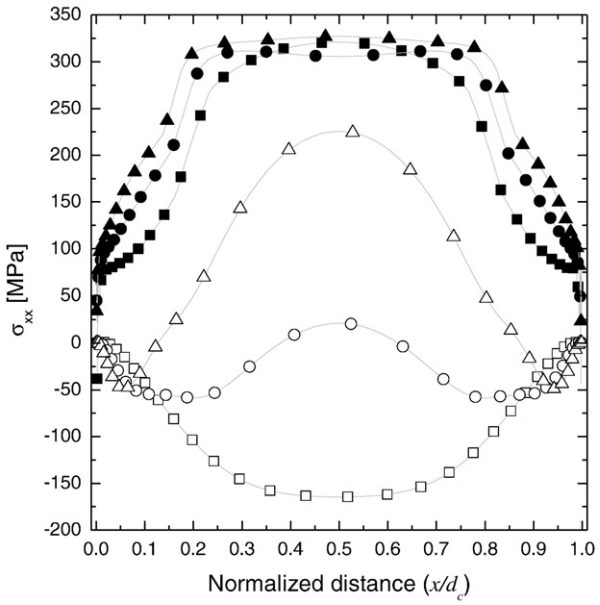

Fig. 7. σ_{xx} stress distribution between two consecutive cracks for the case with the interlayer in the film/substrate interface: unfilled symbols — stress distribution at the film surface; filled symbols — stress distribution at the film/substrate interface; square — $\lambda = 5$; circle — $\lambda = 10$ and triangle — $\lambda = 15$.

this spacing becomes large, the stress distribution becomes flat far from the cracks, such that the maximum tensile value expands over a larger distance of film surface. This point was not reached for the conditions analyzed in this work. For the stresses at the surface, one deviation between analytical and finite element analysis refers to a region of compressive stresses close to the cracks, which are usually seen (Figs. 3-5 and 7) in the finite element analyses [16–21] and are absent in the analytical ones [2,6,13,16].

The differences between analytical and finite element analyses increase as stresses along the interface are considered. In this case, FEM studies show that, different from the assumption made in the analytical models, σ_{xx} stresses at the interface may be significantly more tensile than those at the surface. In some cases [18,19], this fact was associated with a tendency for new cracks to nucleate at the interface. In fact, an example of a crack at the interface was shown by Krishnamurhty and Reimanis [18], who associated the crack with the peak of interfacial tensile stresses mentioned in Section 3.2. Although the same trends of higher stresses at the interface than at the surface were obtained in this work, one must consider that the nucleation of new cracks is not only related to stresses, but also to the size and distribution of defects. Furthermore, the propagation of cohesive cracks in thin films is described by phenomena related to the mechanical properties of the film and the substrate [24].

The results presented in this work indicate that care should be taken also in the preparation of the finite element model, since differences of approximately one order of magnitude may be observed for film stresses, depending on the geometrical and physical parameters selected during model formulation. For example, in the baseline analysis (Fig. 3), the movement of film edges was considerably constrained close to the crack tip, promoting a considerable increase in film stresses, especially at the interface. Much lower stresses were calculated for the entire inter-crack region, and not only to the region close to the cracks, as a stress-relieving phenomenon became possible during the finite element analyses. In this case, this phenomenon was either the plastic deformation of the film (Fig. 4) or of an interlayer between the film and the substrate (Fig. 7). Lower values of film stresses were also obtained with a reduction of the constraints imposed at the crack tip. These lower constraints were obtained when a fully-opened crack (Fig. 5b) was considered, as shown experimentally in the literature [14,18], or by considering a slight debonding of the film/substrate interface (Fig. 5a).

The analyses that allowed stress relieving phenomena provided stress values on the same order of magnitude for the regions far from the cracks. The stress distribution was also similar when comparing the cases with two and three cracks.

5. Conclusions

In this work, a series of 2D finite element analysis was conducted to evaluate four different possibilities of modeling the uniaxial straining of coated systems. The range of mechanical properties considered allowed the following conclusions:

- All analyses of σ_{xx} stresses at film surface provided similar trends, which agree with the analytical and finite element analyses in the literature.
- Significant changes in the absolute values of film stresses at the interface may be obtained depending on the conditions selected in the finite element modeling. Results have shown that the differences refer to the entire distribution of σ_{xx} stresses and not only to those close to the predefined cracks, even in the cases where only the crack geometry was altered in the analysis.
- The values of interface σ_{xx} stresses were more tensile than the stresses at the surface, independent of the geometrical and physical conditions selected in the finite element model preparation.

Acknowledgements

The authors recognize the National Council for Scientific and Technological Development-CNPq for financial support through processes 380172/2010-0 and 303780/2008-8.

References

[1] M.S. Hu, A.G. Evans, Acta Metall. 37 (1989) 917.
[2] D.C. Agrawal, R. Raj, Acta Metall. 37 (1989) 1265.
[3] F.-S. Shieu, R. Raj, S.L. Sass, Acta Metall. 38 (1990) 2215.
[4] P.H. Wojciechovski, S. Mendolia, J. Vac. Sci. Technol. A 7 (1989) 1282.
[5] M. Ignat, in: J.H. Park (Ed.), Chapter 3 in Surf. Eng. Series, Vol. 2, ASM Int. Series, 2001, p. 45.
[6] C.H. Hsueh, M. Yanaka, J. Mater. Sci. 38 (2003) 1809.
[7] P. Scafidi, M. Ignat, J. Adhes. Sci. Technol. 12 (1998) 1219.
[8] A.J. Atanacio, B.A. Latella, C.J. Barbe, M.V. Swain, Surf. Coat. Technol. 192 (2005) 354.
[9] M. Ignat, T. Marieb, H. Fujimoto, P.A. Flinn, Thin Solid Films 353 (1999) 201.
[10] B.A. Latella, B.K. Gan, H. Li, Surf. Coat. Technol. 201 (2007) 6325.
[11] T. Ohmura, S. Matsuoka, Surf. Coat. Technol. 169–170 (2003) 728.
[12] H.-J. Kim, M.-W. Moon, D.-I. Kim, K.-R. Lee, K.H. Oh, Scripta Mater. 57 (2007) 1016.
[13] M. Yanaka, Y. Tsukahara, N. Nakaso, N. Takeda, J. Mater. Sci. 33 (1998) 2111.
[14] E. Harry, A. Rouzaud, M. Ignat, P. Juliet, Thin Solid Films 332 (1998) 195.
[15] R.M. Souza, M. Ignat, C.E. Pinedo, A.P. Tschiptschin, Surf. Coat. Technol. 204 (2009) 1102.
[16] B.F. Chen, J. Hwang, I.F. Chen, G.P. Yu, J.-H. Huang, Surf. Coat. Technol. 126 (2000) 91.
[17] J.L. Beuth, Int. J. Solids Struct. 29 (1992) 1657.
[18] S. Krishnamurthy, I. Reimanis, Surf. Coat. Technol. 192 (2005) 291.
[19] S. Nekkanty, M.E. Walter, R. Shivpuri, J. Mech. Mater. Struct. 7 (2007) 1231.
[20] M. Yanaka, Y. Tsukahara, T. Okabe, N. Takeda, J. Appl. Phys. 90 (2001) 713.
[21] P. Bansal, P.H. Shipway, S.B. Leen, Surf. Coat. Technol. 200 (2006) 5318.
[22] T. Pachler, R.M. Souza, A.P. Tschiptschin, Surf. Coat. Technol. 202 (2007) 1098.
[23] 10th Ed, Metals Handbook, Vol.2, ASM International, 1990.
[24] J.W. Hutchinson, Z. Suo, Adv. Appl. Mech. 29 (1992) 63.
[25] Z.C. Xia, J.W. Hutchinson, J. Mech. Phys. Solids 48 (2000) 1107.
[26] J.L. Beuth, N.W. Klingbeil, J. Mech. Phys. Solids 44 (1996) 1411.
[27] M. Kotoul, O. Sevecek, T. Profant, Eng. Fract. Mech. 77 (2010) 229.